Aust. J. Phys., 1979, **32**, 469–89

Effects of the Wavenumber Spectrum of a Sea Surface on Laser Beam Reflection

D. M. Phillips

Australian Defence Scientific Service, Department of Defence,
Defence Research Centre Salisbury, G.P.O. Box 2151, Adelaide, S.A. 5001.

Abstract

The angular and temporal distributions of energy in the reflection of a pulsed laser beam from a sea surface depend on the diameter of the beam and on the wavenumber spectrum of the water surface. Theoretical expressions are derived for the influence on the reflection of the mean height and slope of waves in the illuminated area as well as the variation of the height and slope within this area. The results are applied to airborne lasers for wave height profiling, altimetry and water depth sounding. The optimum beam diameter depends on both the application and the wavenumber spectrum of the water surface.

1. Introduction

The reflection of a short laser pulse from a sea surface is influenced in several ways by the wavenumber spectrum of that surface:

The mean water level within the illuminated area determines the delay between the time of transmission of the laser pulse and the time of detection of the peak of the reflected pulse. The variation of mean water level in a series of measurements comprises the data used by a wave height profiler. This same variation is also an error that limits the accuracy of an altimeter. Clearly, these two applications require beams of different diameters.

The variation of water level within the illuminated area determines the temporal spread of the reflected pulse. Since this spread slows the pulse risetime, amplitude fluctuations will introduce timing errors when threshold detection is used. A small beam diameter minimizes water level variation within the illuminated spot, but it also increases amplitude fluctuations in the reflected pulse detected by a receiver.

The slope distribution of the sea surface affects the amplitude and variability of the received signal. When a rippled water surface is illuminated by a large diameter laser beam, the reflection is diffuse and the amplitude of the received signal is relatively stable. However, when a long smooth swell is illuminated by a narrow laser beam, the reflection is almost specular and moves around in all directions, producing an occasional bright flash at a fixed observation point. For reliable detection of the reflected pulse, a large beam diameter is therefore preferable.

These and other considerations will sometimes lead to conflicting requirements for the beam diameter. The theoretical study of laser beam reflection from an ocean surface by Swennen (1968) takes no account of the wavenumber spectrum of the sea surface. In the present paper, general expressions are derived for the influence of wavenumber spectra on laser beam reflection, and the results are related to several important applications.

2. Description of Sea Surface

(*a*) *Wave Height Spectrum*

The undulation of a water surface can be described by the height $\zeta(\boldsymbol{r})$ of the water above a point $\boldsymbol{r}$ in the horizontal plane of mean water height. By this definition we have

$$\bar{\zeta} \equiv \int \zeta(\boldsymbol{r})\, \mathrm{d}\boldsymbol{r} = 0 .$$

The surface heights at adjacent points are related by the two-dimensional spatial autocorrelation function

$$Z(\boldsymbol{r}) = \lim_{Q\to\infty}\left\{(\pi Q^2)^{-1}\left(\int \zeta(\boldsymbol{\rho})\,\zeta(\boldsymbol{r}+\boldsymbol{\rho})\,\mathrm{d}\boldsymbol{\rho}\right)_{\rho<Q}\right\}, \tag{1}$$

where $\boldsymbol{\rho}$ is a horizontal position vector. It should be noted that $Z(0)$ is simply the variance of the surface height. The wavenumber spectrum of the water height variance is the Fourier transform of the autocorrelation function, namely

$$\Psi(\boldsymbol{k}) = (2\pi)^{-2}\int Z(\boldsymbol{r})\exp(-\mathrm{i}\,\boldsymbol{k}\,.\,\boldsymbol{r})\,\mathrm{d}\boldsymbol{r}, \tag{2}$$

where $k = 2\pi/\lambda$ is the wavenumber corresponding to the wavelength λ (see e.g. Phillips (1969), equation 4.1.14). Using polar coordinates $\boldsymbol{r} = (r, \alpha)$, a direction-independent wavenumber spectrum is defined by

$$\chi(k) = \int \Psi(k)\, k\, \mathrm{d}\alpha, \tag{3}$$

which differs by a factor k from that used by Phillips (1969, Chapter 4).

(*b*) *Wave Slope Spectrum*

The slope of a water surface at a point $\boldsymbol{r}$ can be defined by the cartesian components

$$s_x = \partial_x \zeta(\boldsymbol{r}) \qquad \text{and} \qquad s_y = \partial_y \zeta(\boldsymbol{r}), \tag{4}$$

from which it follows that $\bar{s}_x = \bar{s}_y = 0$. The spatial autocorrelation function for slope is defined by

$$S_{xy}(\boldsymbol{r}) = \lim_{Q\to\infty}\left\{(\pi Q^2)^{-1}\left(\int s_x(\boldsymbol{\rho})\, s_y(\boldsymbol{r}+\boldsymbol{\rho})\,\mathrm{d}\boldsymbol{\rho}\right)_{\rho<Q}\right\} \tag{5}$$

and the corresponding direction-independent wavenumber spectrum is denoted by $\Sigma_{xy}(k)$. Assuming that orthogonal slopes are statistically independent, it will be convenient to use the wavenumber spectrum of the total slope variance defined by

$$\Sigma(k) = \Sigma_{xx}(k) + \Sigma_{yy}(k). \tag{6}$$

(*c*) *Equilibrium Spectra*

The wavenumber spectrum of wave height takes a simple form when the sea is 'fully aroused'. This occurs when the wind has blown over a fetch and for a duration that are sufficient for the sea to be in equilibrium with the wind. This equilibrium is established when the energy supplied to the waves is lost again as crests break and form patches of foaming white caps or as parasitic capillary waves are generated. Phillips (1969, Section 4.5) derives the functional forms of the wave spectra in the equilibrium range by similarity considerations. When defined by equations (3) and (6) they are

$$\chi(k) = Bk^{-3} \qquad \text{for} \qquad k_0 < k < k_1 \tag{7}$$

and

$$\Sigma(k) = k^2\chi(k) = Bk^{-1} \qquad \text{for} \qquad k_0 < k < k_1, \tag{8}$$

where k_0 and k_1 depend on wind and sea conditions. The lower cutoff wavenumber k_0 is determined by the largest waves present, while the upper cutoff wavenumber k_1 is governed by the shortest capillary waves. These two parameters are used to characterize the wave slope spectrum, rather than the single parameter of mean square slope used by Swennen (1968).

The validity of the functional forms (7) and (8) is supported by measurements of the related frequency spectra. Data from numerous experiments have been assembled by Phillips (1969, Fig. 4.8) and these are supported by more recent data obtained by Peep (1972) and de Leonibus *et al.* (1973). The value of $B = 4{\cdot}6 \times 10^{-3}$ assigned by Phillips (1969) and Wu (1972) was derived from measurements of the slope variance by Cox and Munk (1954*a*).

(*d*) *Wave Statistics*

The statistical distributions of water heights and slopes are also important for a full description of the sea surface, because they go beyond average properties such as variances and spectra. Since the shape of a sea surface results from the superposition of many independent waves generated by winds in different regions, the central limit theorem predicts gaussian distributions for wave height and wave slope.

Experimental measurements of wave height, analysed by Kinsman (1960), reveal a distribution that is approximately gaussian but has a significant skewness. Observed surface slopes, analysed by Cox and Munk (1954*a*), also show an approximately gaussian distribution, but with an appreciable skewness in the windward direction that results in the most probable surface slope being not zero but a few degrees. These departures from gaussian distributions result from nonlinear distortions of the wave components. In the present study, the first-order approximation of a gaussian distribution is assumed, namely the probability

$$p(s_c, s_u) = (2\pi\sigma_c\,\sigma_u)^{-1} \exp\left(-\tfrac{1}{2}\{(s_c/\sigma_c)^2 + (s_u/\sigma_u)^2\}\right), \tag{9}$$

where σ_c and σ_u are the standard deviations of slope in the crosswind and upwind directions respectively.

3. Properties of Limited Area of Sea Surface

The applications of an airborne laser mentioned in the Introduction all involve the reflection of a beam from a limited area of the sea surface. Important properties of the reflection (such as time delay, time spread, direction and amplitude) depend on the nature of the surface of the illuminated area. Expressions are now derived for: the pulse-to-pulse variation of the mean height and mean slope over the illuminated area of water; the variation of the height and slope within this area; the variation of the difference between the central height and mean height.

(a) *Variance of Mean Height*

The mean water height over a circle of radius R centred on the point $\boldsymbol{r}$ is given by

$$\bar{\zeta}_R(\boldsymbol{r}) = (\pi R^2)^{-1}\left(\int \zeta(\boldsymbol{\rho})\,\mathrm{d}\boldsymbol{\rho}\right)_{|\boldsymbol{\rho}-\boldsymbol{r}|<R}. \tag{10}$$

This expression can also be written as the convolution product

$$\bar{\zeta}_R(\boldsymbol{r}) = \zeta(\boldsymbol{r}) * h_R(\boldsymbol{r}) \equiv \int \zeta(\boldsymbol{r}-\boldsymbol{q})\, h_R(\boldsymbol{q})\,\mathrm{d}\boldsymbol{q}, \tag{11}$$

where the averaging function

$$\begin{aligned} h_R(\boldsymbol{r}) &= (\pi R^2)^{-1} \quad \text{for} \quad r < R \\ &= 0 \qquad\qquad\quad\;\; r > R \end{aligned} \tag{12}$$

has the Fourier transform (Ditchburn 1952)

$$H_R(\boldsymbol{k}) = (2\pi)^{-2}\, 2\mathrm{J}_1(kR)/kR. \tag{13}$$

The autocorrelation function for the mean water height is derived by substituting the expression for $\bar{\zeta}_R(\boldsymbol{r})$ in equation (11) in place of $\zeta(\boldsymbol{r})$ in equation (1). This yields

$$\bar{Z}_R(\boldsymbol{r}) = Z(\boldsymbol{r}) * h_R(\boldsymbol{r}) * h_R(-\boldsymbol{r}), \tag{14}$$

which is a generalization of the theorem proved by Papoulis (1962, equation 12-43). It follows that the corresponding wavenumber spectrum is

$$\bar{\Psi}_R(\boldsymbol{k}) = (2\pi)^4\, \Psi(\boldsymbol{k})\, H_R(\boldsymbol{k})\, H_R^*(\boldsymbol{k}), \tag{15}$$

from which the direction-independent form

$$\bar{\chi}_R(k) = \chi(k)\{2\mathrm{J}_1(kR)/kR\}^2 \tag{16}$$

is derived by substituting $H_R(\boldsymbol{k})$ from equation (13).

When the sea is fully aroused, the wavenumber spectrum in equation (7) should be substituted for $\chi(k)$ in equation (16). The autocorrelation function for mean water height

$$\bar{Z}_R(r) = B\int_{k_0}^{k_1} k^{-3}\{2\mathrm{J}_1(kR)/kR\}^2\,\mathrm{J}_0(kr)\,\mathrm{d}k \tag{17}$$

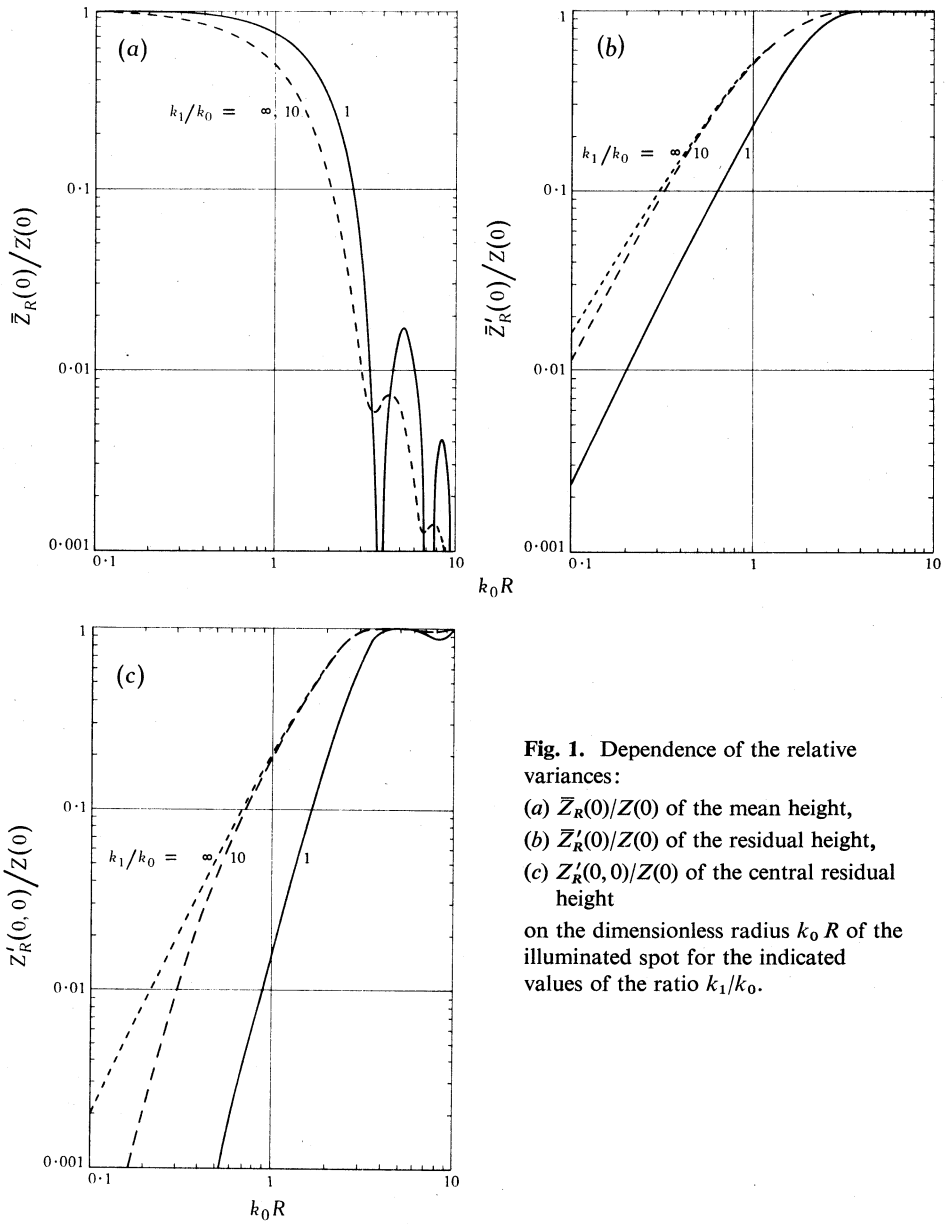

Fig. 1. Dependence of the relative variances:
(*a*) $\bar{Z}_R(0)/Z(0)$ of the mean height,
(*b*) $\bar{Z}'_R(0)/Z(0)$ of the residual height,
(*c*) $Z'_R(0,0)/Z(0)$ of the central residual height
on the dimensionless radius $k_0 R$ of the illuminated spot for the indicated values of the ratio k_1/k_0.

is then obtained from the inverse Fourier transform in polar coordinates

$$Z(r) = \int_0^\infty \chi(k)\, J_0(kr)\, dk\,. \tag{18}$$

It follows that the variance of the mean water height relative to the total height variance is

$$\bar{Z}_R(0)/Z(0) = 2(k_0^{-2} - k_1^{-2})^{-1} \int_{k_0}^{k_1} k^{-3}\{2J_1(kR)/kR\}^2\, dk\,. \tag{19}$$

This ratio is shown in Fig. 1*a* as a function of the dimensionless radius $k_0 R$ of the illuminated spot, the factor k_0 scaling the radius relative to the longest wave present.

It can be seen from Fig. 1*a* that, when the water height is averaged over a small area ($k_0 R \to 0$), the variance of the mean height approaches the total height variance ($\bar{Z}_R(0) \to Z(0)$). This provides some validation of the calculations because no averaging can be achieved with a vanishingly small spot. As the spot becomes larger, however, the averaging becomes more effective and the variance of the mean height is reduced. Indeed, when $k_0 R$ exceeds $\sim 3{\cdot}5$, the mean height variance is only $\sim 1\%$ of the total height variance. The standard error in the mean height, which is the square root of the variance, is then $\sim 10\%$ of the r.m.s. wave height. Further increases in the size of the spot produce only a small additional reduction in the mean height error.

It can also be seen from Fig. 1*a* that the relative variance of mean water height depends primarily on the parameter $k_0 R$ and to a less extent on the ratio k_1/k_0. The significance of the former parameter is more readily apparent when it is expressed as

$$k_0 R = \pi D/\lambda_0 ,$$

where D is the diameter of the spot and $\lambda_0 = 2\pi/k_0$ is the wavelength of the longest significant wave present. The reason for the rapid decrease in the relative variance of the mean water height when $k_0 R \approx \pi$ is that the diameter of the spot exceeds the longest wavelength present and hence the height is averaged over at least one wave in every direction. The insensitivity of the averaging to the ratio k_1/k_0 is due to the strong bias towards short wavenumbers of the wave height spectrum (equation 7). In physical terms, this exemplifies the small contribution to the wave height from ripples.

In the application of a laser (or radar) altimeter, the influence of swell on height measurements can be largely eliminated by making the diameter of the illuminated spot greater than the length of the longest wave likely to be encountered. In the application of a wave height profiler, which determines the water height with a beam of finite diameter, the measured variance will correspond to the quantity $\bar{Z}_R(0)$. Therefore the profiler will record over 90% of the total variance $Z(0)$ for all values of k_1/k_0 if $k_0 R$ is less than $\sim 0{\cdot}3$ (see Fig. 1*a*). In the other words, the profiler will record the height of most of the significant waves if the spot diameter is less than one tenth of the characteristic wavelength of the sea being studied.

(*b*) *Variance of Residual Height*

The residual height of the water surface at the point $\boldsymbol{r}+\boldsymbol{\rho}$ within the averaging circle is defined as

$$\zeta'_R(\boldsymbol{r}, \boldsymbol{\rho}) = \zeta(\boldsymbol{r}+\boldsymbol{\rho}) - \bar{\zeta}_R(\boldsymbol{r}) . \tag{20}$$

The autocorrelation function for the residual water height is derived by substituting the above expression for $\zeta'_R(\boldsymbol{r}, \boldsymbol{\rho})$ in place of $\zeta(\boldsymbol{r})$ in equation (1). With the aid of equations (11) and (14), this yields

$$Z'_R(\boldsymbol{r}, \boldsymbol{\rho}) = Z(\boldsymbol{r}) + \bar{Z}_R(\boldsymbol{r}) - Z(\boldsymbol{r}+\boldsymbol{\rho}) * h_R(\boldsymbol{r}+\boldsymbol{\rho}) - Z(\boldsymbol{r}-\boldsymbol{\rho}) * h_R(\boldsymbol{r}-\boldsymbol{\rho}) . \tag{21}$$

The mean residual autocorrelation over the averaging circle, which is defined by

$$\bar{Z}'_R(r) \equiv (\pi R^2)^{-1}\left(\int Z'_R(r,\rho)\,\mathrm{d}\rho\right)_{\rho<R},$$

reduces to

$$\bar{Z}'_R(r) = Z(r) - \bar{Z}_R(r). \tag{22}$$

Equation (22) is a generalization of the well-known statistical relationship that the sample variance is the difference between the true variance and the variance of the mean. This important result confirms the behaviour expected from qualitative arguments, i.e. that, as the illuminated spot is made bigger, the variation in mean height between measurements is reduced and the variation in height within the spot is increased. Equation (22) shows that the reduction in the former variance equals the increase in the latter.

The ratio of the residual variance of water height averaged over the illuminated area to the total water height variance, namely $\bar{Z}'_R(0)/Z(0)$, is shown in Fig. 1*b* as a function of the dimensionless radius $k_0 R$ of the illuminated spot. It can be seen from Fig. 1*b* that, when the spot is large enough, the average residual height variance $\bar{Z}'_R(0)$ approaches the total height variance $Z(0)$, as would be expected. As the spot becomes smaller, the residual variation within the illuminated area is reduced. Thus, when $k_0 R$ is less than $\sim 0{\cdot}1$, the residual variance is only $\sim 1\,\%$ of the total variance for all values of k_1/k_0.

The broadening of a short laser pulse reflected from the sea surface due to variation in the water height over the illuminated area can be predicted with the aid of Fig. 1*b*. This broadening can introduce timing errors in a wave height profiler when threshold detection of the reflected pulse is employed. Fig. 1*b* shows that, for the resulting height error to be maintained below $10\,\%$ of the r.m.s. wave height, the diameter must be less than $\sim 3\,\%$ of the longest significant wave present (that is, $k_0 R \lesssim 0{\cdot}1$).

(*c*) *Variance of Relative Central Height*

Another important property is the variance of the difference between the water height at the centre of the illuminated spot and the mean height. The autocorrelation function corresponding to this case is given by equation (21) when $\boldsymbol{\rho} = 0$, that is,

$$Z'_R(r,0) = Z(r) + \bar{Z}_R(r) - 2Z(r) * h_R(r),$$

which yields the wavenumber spectrum

$$\chi'_R(k,0) = \chi(k)\{1 - 2\pi H_R(k)\}^2.$$

When the sea is fully aroused, a derivation similar to that used to obtain equation (19) shows that

$$Z'_R(0,0)/Z(0) = 2(k_0^{-2} - k_1^{-2})^{-1} \int_{k_0}^{k_1} k^{-3}\{1 - 2\mathrm{J}_1(kR)/kR\}^2\,\mathrm{d}k. \tag{23}$$

This expression for the variance of the relative water height at the centre of the illuminated spot is depicted in Fig. 1*c*. As expected, the variance of the central point

approaches the total variance as the size of the spot increases. Comparison with Fig. 1*b* shows that the central variance is less than the average variance over the illuminated spot. The reason for this can most easily be perceived by considering a plane as a first approximation to the shape of the water surface within the spot. The mean residual variance over the whole spot is then a measure of the slope of the plane, whereas the central residual variance vanishes because the centre lies in the plane. It follows that the residual variance of the central point is second order and depends on the curvature of the water surface.

Fig. 1*c* is relevant to the application of a laser depth sounder, so designed that it receives a surface reflection from a large spot but has a narrow concentric beam penetrating the water surface. In this case, the residual height error of the central beam is less than (say) 10% of the r.m.s. wave height when

$$Z'_R(0,0)/Z(0) \lesssim 0{\cdot}01\,.$$

Fig. 1*c* shows this condition to be satisfied for $k_0 R \lesssim 0{\cdot}3$, that is, when the diameter of the spot used for the surface reflection is less than 10% of the longest significant wavelength present. Comparison with Fig. 1*a* shows that a requirement for small variance of the mean water height over a spot conflicts with a requirement for small residual variance at the centre.

(*d*) *Variance of Mean Slope*

The derivation of the variance of the mean water height given in Section 3*a* is sufficiently general that it can be applied (with only minor changes) to slopes. By analogy with equation (16), the wavenumber spectrum of the mean slope of the illuminated water surface is

$$\bar{\Sigma}_R(k) = \Sigma(k)\{2\mathrm{J}_1(kR)/kR\}^2\,. \tag{24}$$

For a fully aroused sea, the wavenumber spectrum is given by equation (8). A derivation, similar to that used to obtain equation (19), shows that the variance of the mean surface slope relative to the total slope variance is

$$\bar{S}_R(0)/S(0) = \{\ln(k_1/k_0)\}^{-1} \int_{k_0}^{k_1} k^{-1}\{2\mathrm{J}_1(kR)/kR\}^2\,\mathrm{d}k\,. \tag{25}$$

The dependence of this ratio on the dimensionless parameters $k_0 R$ and k_1/k_0 is shown in Fig. 2*a*.

It can be seen from Fig. 2*a* that, as the spot shrinks to a point ($k_0 R \to 0$), the variance of the mean slope $\bar{S}_R(0)$ of the area approaches the total variance $S(0)$ of the water surface. This asymptotic behaviour is necessary for the wave slope variance (as it is for the wave height variance) and consequently Fig. 2*a* resembles Fig. 1*a* in this respect. Furthermore, when $k_0 R \approx \pi$ and the diameter of the spot approaches the wavelength of the longest significant wave present, the variance of the mean slope falls rapidly for $k_1/k_0 = 1$, as does the variance of the mean wave height in Fig. 1*a*.

However, the parameter k_1/k_0 is much more significant for the mean slope variance than it is for the mean height variance. In other words, the mean slope variance

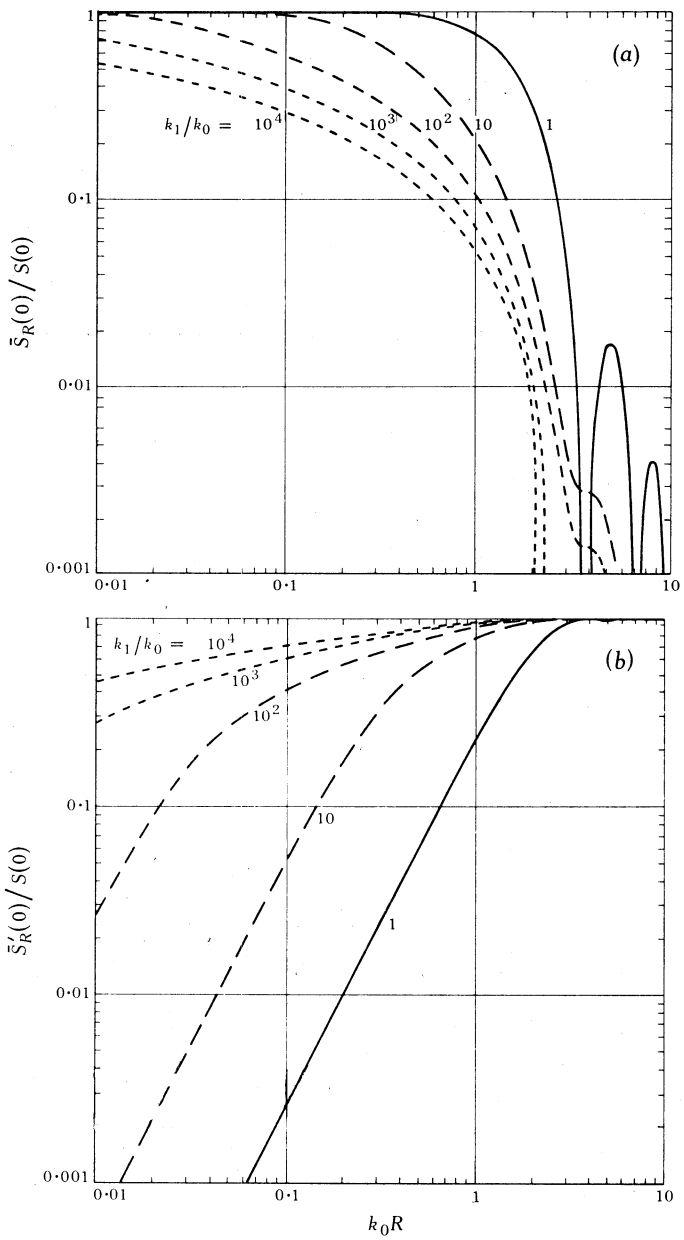

Fig. 2. Dependence of the relative variances:
(*a*) $\bar{S}_R(0)/S(0)$ of the mean slope,
(*b*) $\bar{S}'_R(0)/S(0)$ of the residual slope
on the dimensionless radius $k_0 R$ of the illuminated spot for the indicated values of the ratio k_1/k_0.

is determined by the whole range of wavenumbers contributing to the slope spectrum and not just the low cutoff wavenumber k_0. This difference is due to the functional forms of the wave spectra in the equilibrium range given in equations (7) and (8). Whereas the height spectrum is clearly dominated by small wavenumbers or long wavelengths, the slope spectrum is only weakly biased in that way.

In any application requiring the detection of a laser beam reflected from the sea surface, the strongly directional nature of the reflection can present problems. The reflection will fill a solid angle of a size determined by the roughness of the water surface. The central direction of this solid angle is determined by the mean slope of the illuminated area of water. If both the incident laser beam and the receiving telescope are vertical, the mean slope of the illuminated spot must be small enough for the reflected cone to include the vertical. A small mean-slope variance is therefore necessary but not sufficient for reliable detection of the reflection of a laser pulse from the sea surface.

(*e*) *Variance of Residual Slope*

The residual slope of the water surface at the point $\boldsymbol{r}+\boldsymbol{\rho}$ within the averaging circle is defined by

$$s'_R(\boldsymbol{r}, \boldsymbol{\rho}) = s(\boldsymbol{r}+\boldsymbol{\rho}) - \bar{s}_R(\boldsymbol{r}), \tag{26}$$

which is analogous to the definition of residual height in equation (20). A similar argument shows that the mean autocorrelation function of residual slope is given by

$$\bar{S}'_R(\boldsymbol{r}) = S(\boldsymbol{r}) - \bar{S}_R(\boldsymbol{r}), \tag{27}$$

which is the analogue of equation (22). The ratio $\bar{S}'_R(0)/S(0)$ of the residual slope variance to the total slope variance is shown in Fig. 2*b* as a function of the dimensionless parameters $k_0 R$ and k_1/k_0. It can be seen that the asymptotic behaviour of all the curves is as required, namely the residual slope variance approaches the total slope variance as the size of the illuminated spot increases. The range of wavenumbers, over which the slope spectrum is saturated and which is indicated by the parameter k_1/k_0, is clearly of great importance. Consequently, Fig. 2*b* provides insufficient evidence for deducing the reliability of detection of a laser pulse reflected from a water surface. This question is examined in greater detail in the next section.

4. Laser Beam Reflection from Sea Surface

The reflection of a laser beam from the sea surface is influenced by the properties of the illuminated area of water. These properties are now used to derive the amplitude and variability of the reflected pulse, as well as its time delay and time spread.

(*a*) *Average Amplitude of Reflected Pulse*

The reflection of a diverging beam from an airborne laser is shown schematically in Figs 3*a* and 3*b*. For a transmitted radiant flux F_t, the irradiance at the sea surface on a plane normal to the incident light is approximately

$$E(\phi) = (F_t \cos^2 \phi)/\Omega h^2, \tag{28}$$

where h is the aircraft height, Ω is the solid angle of the diverging beam and ϕ is the nadir angle. It is assumed that the irradiance is uniform within the beam and that the divergence is small.

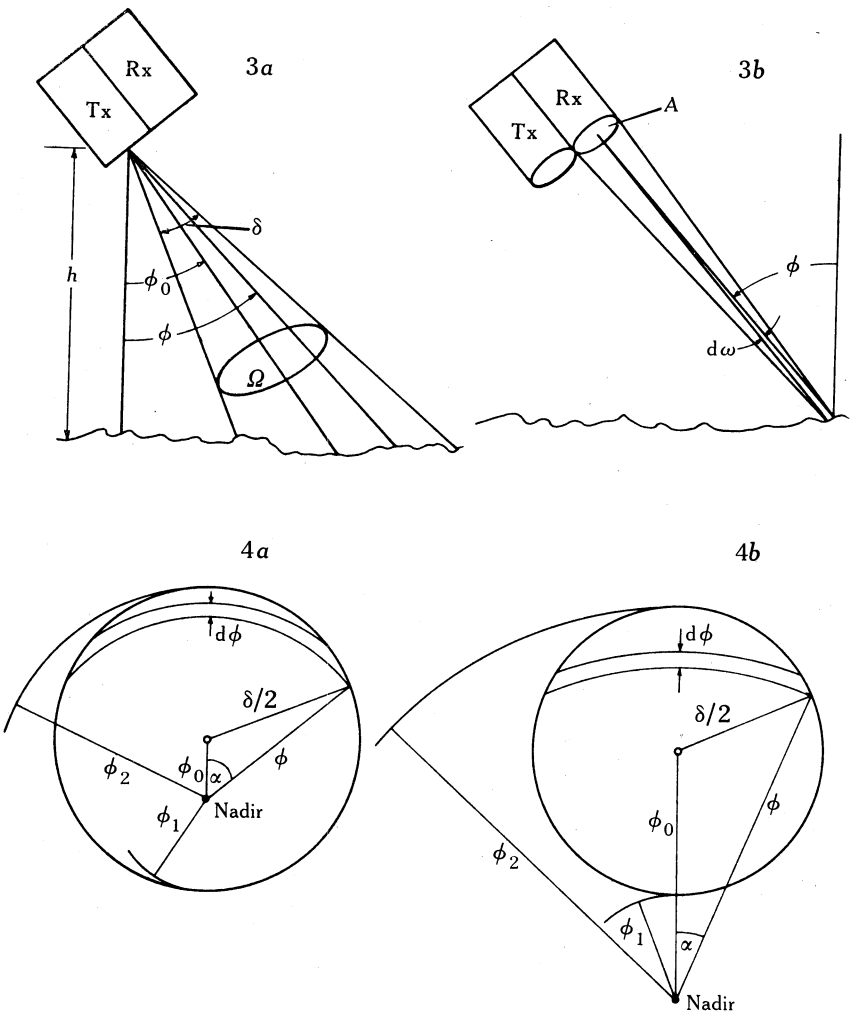

Fig. 3. Schematic diagram of laser beam reflection from a sea surface: (*a*) the transmitter geometry and (*b*) the receiver geometry.

Fig. 4. Geometry of the tilted laser beam and receiver field of view: (*a*) small tilt and (*b*) large tilt.

The radiance $L(\phi)$ reflected from the sea surface at a zenith angle ϕ can be found using the 'scattering cross section' derived from the geometry of reflection from a water surface by Cox and Munk (1954*b*, equation 9). When the receiver is adjacent to the transmitter (as shown in Fig. 3), their result becomes

$$\{L(\phi)\cos\phi\}/E(\phi) = 0{\cdot}25\eta(0)p(\phi)\sec^4(\phi), \tag{29}$$

where $\eta(0)$ is the reflection coefficient at normal incidence and $p(\phi)$ is the probability of the water facet having a tilt at the correct azimuth. The probability given in equation (9) reduces to

$$p(\phi) = (2\pi\sigma^2)^{-1}\exp(-\tfrac{1}{2}\sigma^{-2}\tan^2\phi) \tag{30}$$

when the r.m.s. slopes in the crosswind directions are equal, i.e. when

$$\sigma_c = \sigma_u = \sigma .$$

This simplification introduces only small errors compared with the effects being described in the present theory.

The radiant flux dF_r entering the receiver of area A from the water surface element within the viewing solid angle $d\omega$ is given by

$$dF_r = L(\phi)(Ah^{-2}\cos^2\phi)\{h^2\sec^2\phi\, d\omega\}, \tag{31}$$

where the first factor within braces is the solid angle subtended by the receiver, while the second factor within braces is the projected area of the sea surface element normal to the viewing direction (see Fig. 3). Combining equations (28)–(31) yields the normalized differential reflectance

$$\frac{\Omega}{F_t}\frac{dF_r}{d\omega} = \frac{\eta(0)\,A\sec^3\phi}{4h^2}\,\frac{\exp(-\frac{1}{2}\sigma^{-2}\tan^2\phi)}{2\pi\sigma^2}, \tag{32}$$

which must be integrated to obtain the total received flux.

Equation (32) is integrated over the solid angle within the field of view of the receiver, which is assumed to equal the solid angle of the transmitted beam Ω. This cone has an angular diameter δ and its axis is tilted by an angle ϕ_0 to the nadir, as illustrated in Figs 3 and 4. The sides of the cone nearest to and furthest from the nadir are inclined at the angles

$$\phi_1 = |\tfrac{1}{2}\delta - \phi_0| \qquad \text{and} \qquad \phi_2 = \tfrac{1}{2}\delta + \phi_0 . \tag{33}$$

The solid angle element at the angle ϕ within the field of view is

$$d\omega = 2\alpha(\phi)\,\phi\, d\phi , \tag{34}$$

where

$$\alpha(\phi) = \pi \qquad \text{for} \qquad \phi < \phi_1$$

$$= \arccos\big((\phi_0^2 + \phi^2 - \tfrac{1}{4}\delta^2)/2\phi_0\phi\big) \qquad \phi_1 < \phi < \phi_2 .$$

For tilt angles less than $\frac{1}{2}\delta$ (the small tilt case illustrated in Fig. 4*a*), the integration is between 0 and ϕ_2, while for larger tilts it is from ϕ_1 to ϕ_2 (the large tilt case illustrated in Fig. 4*b*). The ratio of received to transmitted flux can be written as

$$F_r/F_t = \eta(0)\,(A/4h^2\Omega)\,\mathscr{R}(\phi_0, \delta, \sigma), \tag{35}$$

where

$$\mathscr{R}(\phi_0, \delta, \sigma) = \left(\int \sec^3(\phi)\,(2\pi\sigma^2)^{-1} \exp(-\tfrac{1}{2}\sigma^{-2}\tan^2\phi)\, 2\alpha(\phi)\,\phi\, d\phi \right)_{\Omega} \tag{36}$$

is the relative reflectance of the sea surface.

Two limiting cases of the relative reflectance can be evaluated when the beam is vertical ($\phi_0 = 0$, $\alpha = \pi$, $\tan\phi \approx \phi$): Firstly, when the water is calm ($\sigma \to 0$), we have

$$\mathscr{R}(0, \delta, 0) = 1 ,$$

so that, in general, $\mathscr{R}(\phi_0, \delta, \sigma)$ is the amplitude of the reflection relative to that from a mirror. Secondly, when the water is rough ($\sigma \gg \delta$), we have

$$\mathscr{R}(0, \delta, \sigma) = \Omega/2\pi\sigma^2, \tag{37}$$

and equation (35) then reduces to

$$F_r/F_t = \eta(0)\, A/8\pi h^2\sigma^2, \tag{38}$$

which is a useful result for practical applications. It shows that the received signal is independent of the beam divergence, and hence that the most useful quantity to evaluate is the relative signal return $\mathscr{R}(\phi_0, \delta, \sigma)/\Omega$.

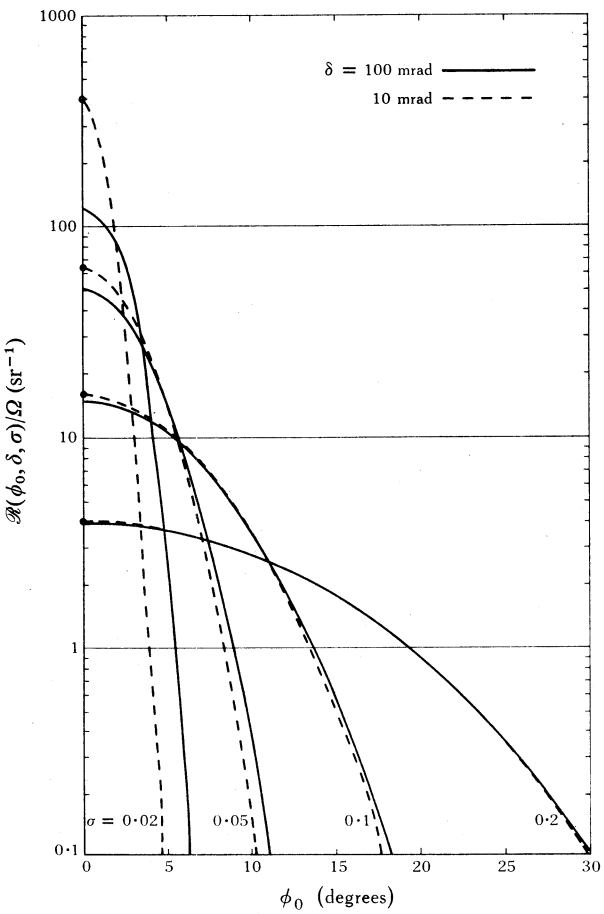

Fig. 5. Dependence of the relative signal return $\mathscr{R}(\phi_0, \delta, \sigma)/\Omega$ on the roll angle ϕ_0 for the indicated values of the beam divergence δ and the r.m.s. residual slope σ.

Fig. 5 shows the dependence of $\mathscr{R}(\phi_0, \delta, \sigma)/\Omega$ on roll angle ϕ_0 for several values of r.m.s. slope σ and beam divergence δ. When the water is rough ($\sigma \approx 0{\cdot}2$) the beam divergence has little effect, and the return signal is relatively insensitive to roll. In calm water, however, a small roll angle can produce an enormous drop in signal.

Under these conditions the beam divergence is significant. The approximate values of the relative signal return determined from equation (36) (which is valid for $\phi_0 = 0$ and $\sigma \gg \delta$) are indicated in Fig. 5 by solid circles on the vertical axis. The agreement between these points and the curves for $\delta = 10$ mrad provides confirmation of the accuracy of the numerical integration used to obtain the curves.

The range of seas observed by Cox and Munk (1954*b*) corresponds to a variation of σ from 0·09 to 0·28. This range of conditions would produce vertical signal returns varying from 2 to 20 sr^{-1}, independent of the beam divergence below 100 mrad. The signal at 15° roll (or scan) angle would drop by a factor of between ~ 2 and ~ 100 over this range of sea states.

(*b*) *Variability in Amplitude of Reflected Pulse*

In the preceding subsection, the calculation of the received pulse amplitude assumed the average slope over the illuminated area to be zero, i.e. Fig. 5 provides only the average amplitude of the signal return. Fluctuations in this amplitude due to the passage of waves are equally important and these are now examined. Swell causes fluctuations in the average slope that depend on the diameter of the illuminated spot and on the wavenumber spectrum of the sea surface. These slope fluctuations induce fluctuations in the amplitude of the received pulse because of changes in the reflection geometry.

When the transmitter and receiver are vertical but the mean slope of the illuminated surface is $\bar{s}$, the reflection geometry is equivalent to a horizontal mean sea surface illuminated by a beam inclined at an angle ϕ_0, where $\tan\phi_0 = \bar{s}$. The amplitude of a pulse reflected from an inclined surface can therefore be read from Fig. 5 or calculated from equation (36).

When a threshold detector is used to detect pulses of variable amplitude, it is important to know the probability that the pulse amplitude exceeds the threshold. It can be seen from Fig. 5 that the probability of the relative signal return exceeding $\mathscr{R}(\phi_0, \delta, \sigma)/\Omega$ equals the probability that $\bar{s} < \tan\phi_0$. Assuming an isotropic gaussian distribution, the probability of a mean slope $\bar{s}$ at any azimuth is

$$p(\bar{s}) = \bar{s}\bar{\sigma}^{-2}\exp(-\tfrac{1}{2}\bar{s}^2/\bar{\sigma}^2), \tag{39}$$

where $\bar{\sigma}$ is the r.m.s. mean slope (cf. equation (30) at a particular azimuth). Integration and inversion yields

$$\phi_0 = \arctan\bigl(\bar{\sigma}(\ln q^{-1})^{\frac{1}{2}}\bigr), \tag{40}$$

where q is the 'failure' probability, i.e. the probability that the mean slope exceeds $\tan\phi_0$ and the pulse amplitude is below threshold.

The threshold signal returns that correspond to different failure probabilities can be determined from equation (36) or from Fig. 5 with the aid of equation (40). The results for a failure probability of 1 % are presented in Fig. 6*a*. It can be seen that the threshold must be set considerably lower than the peak signal return if reliable detection is to be achieved over a wide variety of sea conditions.

The threshold signal returns in the absence of swell and the absence of aircraft roll are given in Fig. 6a by the curves for $\bar{\sigma} = 0$. These threshold curves are identical for all failure probabilities because there is no variation in the amplitude of the

reflected pulse when the mean slope over the illuminated area remains zero. Furthermore, these threshold curves correspond to the signal returns shown in Fig. 5 when $\phi_0 = 0$, that is, in the absence of aircraft roll. This follows from the fact that Fig. 5 was produced with the assumption of a zero mean slope ($\bar{\sigma} = 0$).

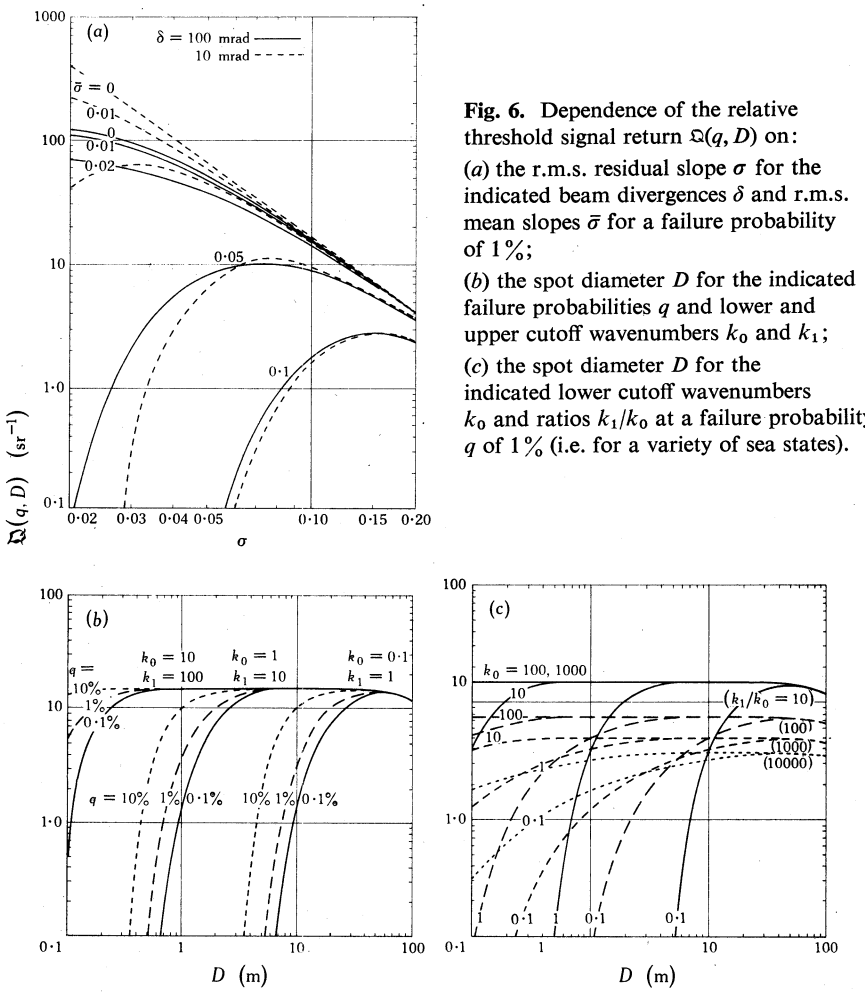

Fig. 6. Dependence of the relative threshold signal return $\Omega(q, D)$ on:
(*a*) the r.m.s. residual slope σ for the indicated beam divergences δ and r.m.s. mean slopes $\bar{\sigma}$ for a failure probability of 1%;
(*b*) the spot diameter D for the indicated failure probabilities q and lower and upper cutoff wavenumbers k_0 and k_1;
(*c*) the spot diameter D for the indicated lower cutoff wavenumbers k_0 and ratios k_1/k_0 at a failure probability q of 1% (i.e. for a variety of sea states).

Each set of threshold curves in Fig. 6a for a fixed beam divergence shows a fall to lower values as the r.m.s. mean slope increases. This is because the amplitude of the reflected pulse in the vertical direction becomes more variable as the swell increases and tilts the reflected cone further away from the zenith. The reduction in the threshold is greatest when the reflected cone has a small solid angle, i.e. when the r.m.s. residual slope within the illuminated spot is small.

Beam divergence is significant when the r.m.s. residual slope is small, i.e. when the water surface is relatively smooth within the illuminated spot. Under these conditions, and in the absence of swell ($\bar{\sigma} = 0$), a higher threshold is obtained with a small beam divergence. This is because smooth horizontal water reflects a laser pulse into a narrow vertical cone, which is collected efficiently by the receiver when the

divergence δ of the transmitted beam is smaller than the divergence σ of the reflected cone. When $\delta > \sigma$, the outer parts of the transmitted beam are reflected away from the receiver and are thus wasted. A lower threshold is then required for reliable detection.

If, however, as the swell grows in magnitude the water surface remains smooth ($\bar{\sigma}$ increases for σ small), the situation is reversed: a higher threshold is obtained with a large beam divergence. The collection efficiency with a large beam divergence ($\delta > \sigma$) is still small but, as the directions of the reflected cones from small patches of water within the illuminated spot are 'wobbled' by swell, some parts of the beam still reach the receiver. With a small beam divergence, the reflected cone from a small illuminated spot has a greater probability of missing the receiver altogether—hence the lower threshold.

The curves in Fig. 6*a* are sufficient to predict a satisfactory threshold signal if the spot size is known and if the r.m.s. mean slope over that spot and the r.m.s. residual slope within it are known. Since such information is not always available, additional assumptions must be made.

When the sea is fully aroused and the slope spectrum is saturated between the lower and upper cutoff wavenumbers k_0 and k_1, the variability of the reflected pulse can be analysed further. The relative threshold signal is now redefined as

$$\mathfrak{Q}(q, D) = \mathscr{R}(\phi_0, \delta, \sigma)/\Omega, \tag{41}$$

where q is the failure probability and $D = 2\mathscr{R}$ is the diameter of the illuminated spot. This definition is possible because, for given values of k_0 and k_1, the relative threshold signal is a function of q and D only, as is now shown. The solid angle of the transmitted beam is

$$\Omega = \tfrac{1}{4}R\delta^2, \tag{42}$$

as may be seen from Fig. 3a, and the angular diameter of the beam is

$$\delta = D/h \sec \phi_0. \tag{43}$$

In the ensuing calculations it is assumed that $h = 500$ m and $\phi_0 = 0$. From equation (27) it follows that

$$\sigma^2(D) = \bar{S}'_R(0) = B\ln(k_1/k_0) - \bar{\sigma}^2(D), \tag{44}$$

where the total slope variance is obtained by integrating equation (8). The value $B = 4{\cdot}6 \times 10^{-3}$ assigned by Phillips (1969) and Wu (1972) is used in the present calculations. Finally, from equation (25) we have

$$\bar{\sigma}^2(D) = \bar{S}_R(0) = B \int_{k_0}^{k_1} k^{-1}\{2\mathrm{J}_1(kR)/kR\}^{-2}\,\mathrm{d}k. \tag{45}$$

This establishes the validity of the functional form of $\mathfrak{Q}(q, D)$ in equation (41).

Fig. 6*b* shows the threshold relative signal return $\mathfrak{Q}(q, D)$ as a function of the diameter of the illuminated spot for the failure probabilities $q = 0{\cdot}1\%$, 1% and 10%. Three sets of curves are shown, all for slope spectra covering one decade of wavenumbers, but with different lower cutoff wavenumbers $k_0 = 0{\cdot}1$, 1 and 10 m^{-1}.

These curves were computed from equations (36) and (41), expressed in terms of q, D, k_0 and k_1 with the aid of equations (42)–(45). However, the curves for $q = 1\%$ can be determined graphically from Figs 2*a* or 2*b* and Fig. 6*a*. From given values of k_0, k_1 and D, we can calculate the dimensionless parameters $k_0 R$ and k_1/k_0, which yield σ and $\bar{\sigma}$ from Figs 2*a* and 2*b*. Then, depending on the value of q, Fig. 6*a* will yield the appropriate threshold signal.

It can be seen from Fig. 6*b* that, when the diameter of the spot is large enough, all the curves have the same asymptote, which is constant until D exceeds ~ 20 m. This common asymptote is due to the common value of k_1/k_0 ($= 10$), and hence the common value of the r.m.s. total slope. When the diameter becomes large enough, the r.m.s. mean slope $\bar{\sigma}$ approaches zero, and the threshold signal (see Fig. 6*a*) for a given value of σ depends on the beam divergence δ only. Fig. 6*a* clearly shows that increasing beam divergence reduces the threshold return when $\bar{\sigma} = 0$ (particularly when σ is small). This accounts for the fall in the asymptotic threshold in Fig. 6*b* when the diameter of the spot exceeds ~ 20 m.

Fig. 6*b* shows that the diameter of the illuminated spot needed to achieve a given threshold return depends markedly on k_0. More specifically, the thresholds begin to fall in every case when the spot diameter becomes less than the longest significant wave present ($k_0 D \lesssim 2\pi$).

The acceptable failure probability is also a significant parameter. For example, when the slope spectrum is saturated over the range 1–10 m^{-1}, a spot diameter of 1 m produces a 10% failure level with a threshold return of 10 sr^{-1}. In order to improve the reliability to a failure level of 0·1%, it is necessary either to reduce the threshold by an order of magnitude or to increase the spot diameter by a factor of $\sim 2{\cdot}5$.

The range of wavenumbers over which the slope spectrum is saturated has a significant influence on the threshold as shown in Fig. 6*c*. All the curves correspond to a failure probability of 1%. It can be seen that the asymptotic threshold falls as the saturation range (k_1/k_0) becomes larger. In other words, as the sea becomes rougher the reflection becomes more diffuse and hence less intense in the vertical direction.

The fall in threshold when the spot diameter becomes less than the longest significant wave present ($k_0 D \lesssim 2\pi$), which was noted in Fig. 6*b*, is also evident in Fig. 6*c*. However, the fall is much more rapid when the slope spectrum is saturated over only a small range. When the saturated range is large, due to the presence of many ripples, the threshold is not very sensitive to the size of the illuminated spot.

The above results are presented differently in Fig. 7. By using k_0 and k_1 as axes, each point in the plane corresponds to a particular sea state. The small lower cutoff wavenumbers to the left of the graph correspond to the long wavelength swell of the open ocean, while the large lower cutoff wavenumbers to the right of the graph represent the small waves of restricted waters such as rivers and bays. On the vertical axis, the large upper cutoff wavenumbers towards the top of the graph represent the small ripples generated in a strong wind, while the small upper cutoff wavenumbers towards the lower part of the graph represent smooth waves that occur in calm air. A variety of sea conditions can therefore be represented by an area of the graph.

The restrictions on the illuminated spot diameter D and the threshold signal level needed to achieve failure probabilities less than 1% are depicted in Fig. 7. For a

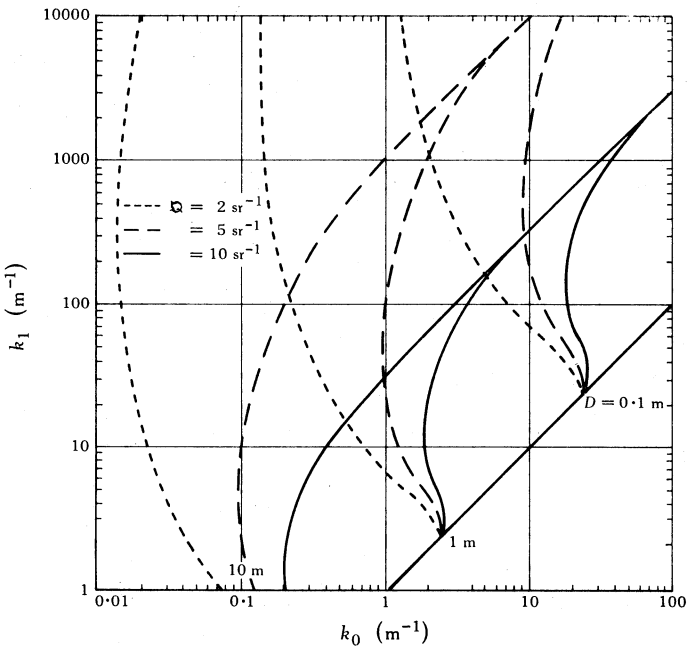

Fig. 7. Range of sea states for which given spot diameters D and relative thresholds Ω achieve a failure probability below 1%.

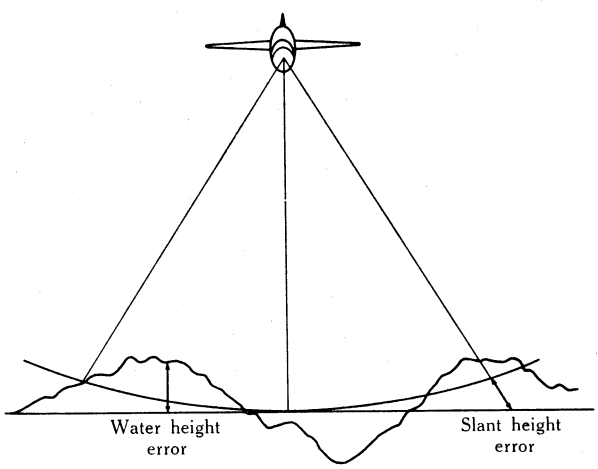

Fig. 8. Variation of water height and slant height errors over the illuminated spot.

given threshold and diameter, the failure probability is below the required value (1%) to the right of the corresponding curve. For a threshold of 10 sr^{-1}, reliable detection is achieved only when the saturated range of wavenumbers k_1/k_0 is less than 30. As the spot diameter is increased, reliable detection is achieved in the presence of longer swells. The effect of reducing the threshold (e.g. with a more sensitive detector) is to achieve reliable detection when the wave spectrum is saturated over a

greater range of wavenumbers. If reliable detection is required over a wide range of upper cutoff wavenumbers and with lower cutoff wavenumbers as small as $0{\cdot}1\ \mathrm{m}^{-1}$, a diameter between 1 and 10 m is required together with a threshold of less than $2\ \mathrm{sr}^{-1}$.

(*c*) *Water Height Resolution*

The time spread of a laser impulse reflected from the sea surface is determined both by the variation of water height within the illuminated area and by the variation of the slant height travelled by the beam. This is illustrated in Fig. 8. The accuracy of a water height measurement is limited by the sum of these two errors and hence by the sea state and the diameter of the illuminated spot.

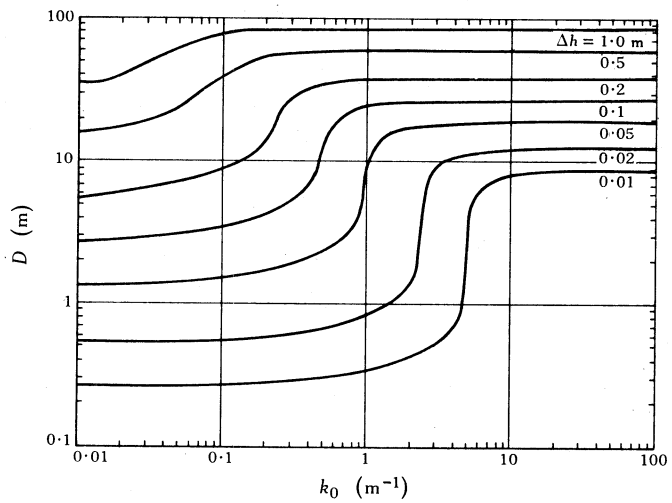

Fig. 9. Dependence of the r.m.s. residual height error Δh on the laser spot diameter D and the sea state (exemplified by the lower cutoff wavenumber k_0).

The variance of the residual water height, which can be derived from equations (19) and (22), is given by

$$\tfrac{1}{2}B(k_0^{-2} - k_1^{-2})\bar{Z}'_R(0)/Z(0)\,. \tag{46}$$

The slant height error of a beam at a zenith angle ϕ from an aircraft at height h is $h(\sec\phi - 1)$. In the small angle approximation, when the square of this error is averaged over an area of diameter D, a variance for the slant error of

$$D^4/192h^2 \tag{47}$$

is obtained. The total r.m.s. height error is therefore

$$\Delta h = \{\tfrac{1}{2}B(k_0^{-2} - k_1^{-2})\,\bar{Z}'_R(0)/Z(0) + D^4/192h^2\}^{\frac{1}{2}}\,. \tag{48}$$

The upper limit of this error, which occurs for $k_1 \gg k_0$, is shown in Fig. 9 as a function of k_0 and D.

In calculating the value of Δh it is assumed that the aircraft altitude is 500 m and that the axis of the transmitted beam is vertical. When k_0 is large, the first term in equation (48) is negligible and the height error is proportional to D^2. In this limit, only small waves are present and the slant height error dominates. When k_0 is small, the first term in equation (48) dominates. It can be shown that, in this limit, the height error is proportional to D. In the presence of strong swell, therefore, wave height errors are larger than slant height errors except for very large diameter spots.

5. Discussion of Applications

An airborne system (such as an altimeter, wave height profiler or water depth sounder) that relies for its operation on the detection of a laser pulse reflected from the sea surface has several system parameters available for optimization. One is the aircraft operating height, but this is often determined by other considerations. Another is the peak output power of the laser pulse, but this may be limited by the laser design. Yet another is the vertical stabilization of the laser beam against pitch and roll variations of the aircraft. Apart from the latter, the only system parameter available for optimization in practice may be the diameter of the illuminated laser spot on the sea surface, which is controlled by the divergence of the transmitted laser beam.

The theory of laser beam reflection developed in the previous sections has been concerned with the influence of laser spot diameter on the accuracy and reliability of surface detection. The reliability is affected by fluctuations in the amplitude of the received pulse, due to variations in the mean slope and surface roughness of the illuminated spot. The accuracy is affected by pulse broadening due to water height variations within the illuminated spot and by pulse-to-pulse timing variations due to swell. The choice of a suitable spot diameter depends on both the application and the range of sea conditions expected.

The theory described in this paper has been developed on the assumption that the wave slope spectrum of the sea is saturated between two cutoff wavenumbers. Unfortunately, experimental data to test the validity of this assumption are lacking. Moreover, the lack of experimental data precludes any detailed predictions. Cutoff wavenumbers can be deduced from slope variance data, but vastly different results are obtained depending on the assumptions employed. Here, therefore, different applications can be discussed only in general terms.

A wave height profiler must illuminate a spot that is small enough to profile the waves but large enough for reliable detection of the reflected signal. The optimum diameter will depend on the wavenumber of the longest waves present, the height resolution required and the maximum failure probability that can be tolerated. Fig. 7 provides the information necessary to determine the optimum diameter.

An altimeter, required to measure height above mean sea level, must illuminate a spot that is large enough for reliable detection of the reflected signal, large enough to measure the mean sea level, but small enough to contain slant height errors. The optimum diameter will be much greater than that required by a wave height profiler. Figs 1 and 7 provide the necessary information.

A water depth sounder, which uses the mean sea level as a reference surface, requires a spot that is large enough for reliable detection of the reflected signal but small enough for adequate accuracy in the height measurement. The large spot suitable for an altimeter may not establish the mean sea level with sufficient precision for use

as a reference in depth sounding. On the other hand, the small spot suitable for a high resolution wave height profiler may compromise the high detection reliability needed by a water depth sounder. Consequently, the optimum diameter for an airborne depth sounder may lie between the other two. Again, Fig. 7 provides the relevant information.

6. Conclusions

The reflection of a pulsed laser beam from a limited area at the sea surface has been analysed theoretically. Temporal and amplitude fluctuations are shown to depend on the wavenumber spectrum of the sea surface. Using a two parameter characterization of the wavenumber spectrum, an expression ((41) with (36)) has been obtained for the probability of the reflected signal failing to exceed a given threshold in the detecting system. Results calculated from this expression, which are presented graphically, allow the optimum diameter of the illuminated spot on the sea surface to be determined for a given application. The main hindrance to the immediate application of these results is the lack of experimental measurements of the two parameters on which the theory is based. When the necessary data become available, the results can be used in applications of lasers for wave height profiling, altimetry and water depth sounding.

Acknowledgment

The author wishes to acknowledge with gratitude the assistance of Miss L. P. Hortin in running numerous computer programs to obtain the results and in plotting most of the graphs.

References

Cox, C., and Munk, W. (1954*a*). *J. Mar. Res.* **13**, 198.
Cox, C., and Munk, W. (1954*b*). *J. Opt. Soc. Am.* **44**, 838.
Ditchburn, R. W. (1952). 'Light' (Blackie: London).
Kinsman, B. (1960). Chesapeake Bay Inst., Johns Hopkins Univ., Tech. Rep. No. 19.
de Leonibus, P. S., *et al.* (1973). *J. Geophys. Res.* **78**, 2650.
Papoulis, A. (1962). 'The Fourier Integral and its Applications' (McGraw–Hill: New York).
Peep, M. (1972). *IEEE Trans. Geosci. Electron.* **10**, 24.
Phillips, O. M. (1969). 'The Dynamics of the Upper Ocean' (Cambridge Univ. Press).
Swennen, J. P. J. W. (1968). *J. Opt. Soc. Am.* **58**, 47.
Wu, J. (1972). *Phys. Fluids* **15**, 741.

Manuscript received 14 December 1978